

Fabrication of nanofiltration membranes via stepwise assembly of oligoamide on alumina supports:
Effect of number of reaction cycles on membrane properties

Original

Fabrication of nanofiltration membranes via stepwise assembly of oligoamide on alumina supports: Effect of number of reaction cycles on membrane properties / Amelio, Antonio; Sangermano, Marco; Kasher, Roni; Bernstein, Roy; Tiraferri, Alberto. - In: JOURNAL OF MEMBRANE SCIENCE. - ISSN 0376-7388. - 543:(2017), pp. 269-276.
[10.1016/j.memsci.2017.08.067]

Availability:

This version is available at: 11583/2680447 since: 2017-09-16T10:19:03Z

Publisher:

Elsevier B.V.

Published

DOI:10.1016/j.memsci.2017.08.067

Terms of use:

This article is made available under terms and conditions as specified in the corresponding bibliographic description in the repository

Publisher copyright

(Article begins on next page)

Fabrication of Nanofiltration Membranes via Stepwise Assembly of Oligoamide on Alumina Supports: Effect of Number of Reaction Cycles on Membrane Properties

Antonio Amelio^a, Marco Sangermano^b, Roni Kasher^c, Roy Bernstein^c, Alberto

Tiraferri^{a,*}

^aDepartment of Environment, Land and Infrastructure Engineering (DIATI), Politecnico di Torino, Corso Duca degli Abruzzi 24, 10129, Torino, Italy

^bDepartment of Applied Science and Technology (DISAT), Politecnico di Torino, Corso Duca degli Abruzzi 24, 10129, Torino Italy

^cDepartment of Desalination and Water Treatment, Zuckerberg Institute for Water Research, Jacob Blaustein Institute for Desert Research, Ben-Gurion University of the Negev, Midreshet-Ben Gurion, Sede Boqer, Israel

*alberto.tiraferri@polito.it; Corso Duca degli Abruzzi 24, 10129, Torino, Italy; Tel. +390110907628, Fax: +390110907699

Abstract

This study presents the preparation procedure and the properties of nanofiltration membranes fabricated by step-by-step assembly on ultrafiltration supports. This procedure allows the covalent binding of molecular layers of alternating monomers, trimesoyl chloride and m-phenylenediamine, to control film growth and surface chemical functionality. The molecular layers are attached directly onto aminated alumina supports, obtained by functionalization of the supports using an aminosilane reagent, for the first time without the need of an anchoring polymeric layer. The membranes are fabricated by performing different numbers of reaction cycles between the two monomers and are characterized along the various cycles (2 to 6.5 reaction cycles). Surface analyses demonstrate the development of the layered assembly and the attained functionalizations as a function of exposed moiety. Electron microscopy proves that low number of cycles allows achievement of a smooth film, while layer thickness and heterogeneity increase above five step reactions. The water permeance and the salt rejection capabilities of the fabricated membranes are in the range of nanofiltration, with observed rejections of 20-80% and 20-95% for NaCl and MgSO₄, respectively. The transport properties correlate well with the number of reaction cycles, thus allowing tuning of the membrane permeance and selectivity by adjusting the total number of layers in the assembly.

Highlights:

- Nanofiltration membranes fabricated by stepwise monomeric assembly
- Surface properties depend on the reaction cycles and on the last reacting monomer
- Number of reaction cycles correlates with membrane transport performance
- More reaction cycles yield membranes with lower permeance and higher selectivity
- Membrane behavior may be tuned by performing a certain number of reaction cycles

Keywords: polyamide; molecular layer-by-layer (mLbL); TFC membranes; nanofiltration; oligoamide.

1. Introduction

Efficient treatment of contaminated water and industrial filtration of organic streams require well-designed stable materials that can effectively separate pollutants. Currently, membrane-based processes of reverse osmosis (RO) and nanofiltration (NF) are successfully applied for organic solvent filtration and to obtain safe water from sources that are loaded with dissolved solids and other hazardous substances (e.g., seawater, wastewater) [1-6]. Thin-film composite (TFC) membranes made of aromatic polyamide on polymeric supports are the state-of-the-art materials for these processes [2].

Traditionally, polyamide selective layers are fabricated by interfacial polymerization, where a diffusion-controlled reaction occurs between two monomers dissolved in two immiscible solvents [7, 8]. The final film functionality and separation properties are the result of mechanisms that are strongly dependent on interconnected parameters (e.g., monomer diffusivity, monomer solubility and reactivity, solvent viscosity, surface tension, environmental conditions) and causing rapid cross-linking of the polyamide layer [9-11]. If not suitably controlled, the interfacial polymerization approach in its nature leads to difficulties in optimizing the desired polyamide properties that would allow maximization of flux and rejection. Also, traditional interfacial polymerization methods give rise to rough polyamide surfaces prone to foulant attachment [1]. Membrane performance is a direct function of the active film thickness, surface roughness, homogeneity of chemical network structure, and functionality, which can be achieved for TFC polyamide membranes by additional post-fabrication treatments [12-18].

Recently, a considerable body of literature has become available around alternative approaches to fabricate TFC membranes for RO and NF [4, 19-21]. For example, roughness of the polyamide membrane was reduced by using ionic liquids as the organic reaction medium during interfacial polymerization [22]. Another promising strategy is based on stepwise or molecular layer-by-layer (mLbL) synthesis of the polyamide or oligoamide active film, during which layers are made to

covalently react one after the other. This procedure was first applied on a non-porous support of gold, allowing the fabrication of a model surface layer mimicking the polyamide layer of RO membranes and exhibiting surface properties comparable to classic aromatic polyamide films [23, 24]. Indeed, other robust studies on model mLbL oligoamide films suggested that this strategy allows high tunability of the surface chemistry [10]. Therefore, this procedure was recently adapted for the fabrication of polyamide and oligoamide films on porous supports, to obtain membranes suitable for filtration applications.

NF membranes were fabricated on polysulfone supports via layer-by-layer interfacial polymerization between amine-rich poly(ethyleneimine) (PEI) chains and trimesoyl chloride (TMC), a triacid monomer [25]. Studies using monomers to form active films have traditionally based their approach on pre-deposition of polyelectrolytes (poly(ethyleneimine) and poly(acrylic acid)) on the porous support; this step was followed by either mLbL assembly of reactive monomers, or classic interfacial polymerization between TMC and m-phenylenediamine (MPD) or other diamine monomers [26-28]. All the previously mentioned methods suffer from important limitations. For example, they involve the use of polymers either during reaction or as a coating of the porous support to initiate the formation of the selective film, thus introducing additional steps and complexity to the overall synthesis. Furthermore, polyelectrolytes are deposited on the support layers with no chemical linkage, which might limit the stability and robustness of the active film. The stability of this layer is essential in processes involving the permeation of water from the support side to the active side, such as use of backwash cleaning, during which the polyelectrolyte layers may detach from the support. Finally, a systematic understanding of how the number of cycles influences membrane properties is still lacking.

This research aims to contribute to this growing area of research by discussing functional membranes fabricated by molecular step-by-step assembly (mLbL) directly on an alumina ultrafiltration support. The term “oligoamide” is used throughout the paper to refer to this film

synthesized by stepwise reaction with limited number of cycles, and to distinguish it from polyamide traditionally synthesized by a polymerization reaction. The decision to use alumina supports was based on the hypothesis that oligoamide monomers can be easily anchored by covalent bonds onto the aminated supports, without the need of middle polymeric layers. Another major advantage of using this inorganic material is its high resistance to harsh chemical conditions, unlike most polymeric supports. The film is grown from the support by alternating coupling reactions of TMC and MPD monomers. This study therefore sets out to assess the effect of number of cycles and of terminating monomer on membrane surface and separation properties. The materials are characterized during the various cycles of film formation: surface chemistry, layer morphology, water fluxes, and rejection of common monovalent and divalent salts are thus fully quantified. The main hypothesis that will be tested is that membrane properties can be tuned by carrying out a desired number of steps during mLbL assembly.

2. Experimental Section

2.1 Materials

Whatman® Anodisc inorganic alumina filter membranes with a diameter 47 mm and nominal pore size of 0.02 μm (as reported by the manufacturer) were used as support in all the fabrications. Sulfuric acid (95-97%, Merck) and hydrogen peroxide (30 w/w%, Sigma-Aldrich) were used to perform piranha pre-treatment of the alumina support. To create an anchoring layer on the support by silanization, ethanol ($\geq 99\%$), acetic acid (99.5 %), and (3-aminopropyl)triethoxysilane (APTES, $\geq 98\%$) were employed. Layered synthesis was carried out using m-phenylenediamine (MPD, 99%), trimesoyl chloride (TMC, 98%), anhydrous dichloromethane (DCM), anhydrous toluene, and triethylamine ($\geq 99\%$). All these chemicals were purchased from Sigma-Aldrich. Deionized (DI) water was obtained from a Milli-Q purification system.

To estimate the molecular weight cutoff (MWCO) of the alumina support, colloidal silica (Ludox HS-40 and Ludox TM-50 purchased from Sigma-Aldrich) dispersed in water was filtered through the membrane. The rejection of the final membranes was evaluated by filtration of MgSO_4 ($\geq 99\%$, Merck) and NaCl (99.8% , Chem-Lab NV).

2.2 Protocol for Molecular Layered Synthesis of Oligoamide

Membranes were synthesized according to the following procedure consisting of four main stages, as depicted in Figure 1:

A. To begin the process, alumina supports were pre-treated for 30 min in a UV-ozone chamber followed by soaking in piranha solution (sulfuric acid: H_2O_2 3:1 v/v) for 1 min to activate the aluminum hydroxide groups (Al-OH). The supports were then rinsed thoroughly with deionized water.

B. Following activation, a silanization reaction to obtain an anchoring amine-terminated layer was conducted at 50°C for 21 hr, in a well-mixed solution (approximately 100 mL for each support) comprising a mixture of ethanol and water (ethanol: water 5:1 v/v), 100 μL of acetic acid, and 4 mL of APTES. The supports were then rinsed in ethanol, dried in an oven for 6 hr at 80°C , and washed again with ethanol before a final curing step in the oven for 2 hr at 80°C .

C. The silanized supports were soaked in toluene containing 1% v/v of triethylamine for 10 min with moderate shaking, and then rinsed with ethanol and dried. The oligoamide synthesis started by washing the supports and all glassware with DCM. Then, each support was placed in a solution of 1 wt% TMC in DCM, in which triethylamine was added to a final concentration of 20 mM. This first reaction between TMC monomers and the silanized support was prolonged for 30 min with mild mixing. This reaction provided the first half cycle of synthesis (0.5), with the seeding layer of TMC covalently anchored by amide bonds to the aminosilane-functionalized alumina support.

D. At the end of the previous stage, the membrane was rinsed in two acetone baths in series and two toluene baths in series, and then placed into a solution of 1 wt% MPD in toluene, to induce the reaction between the monomeric layer of TMC and the MPD monomers for 15 min, with mild mixing. Following this stage (full cycle of synthesis, cycle 1), the membrane was washed in two acetone baths and two DCM baths in series. The following reaction with TMC (cycle 1.5) was conducted as described in (C) but for 15 min. From this point onwards, all the MPD-TMC (steps C and D) reactions were cycled for 15 min each and for a pre-determined total number of times, to allow for growth of the layer one monomer at a time.

As a final stage, the membranes were immersed in water for 10 min. All the membranes were washed with ethanol and kept dry before use.

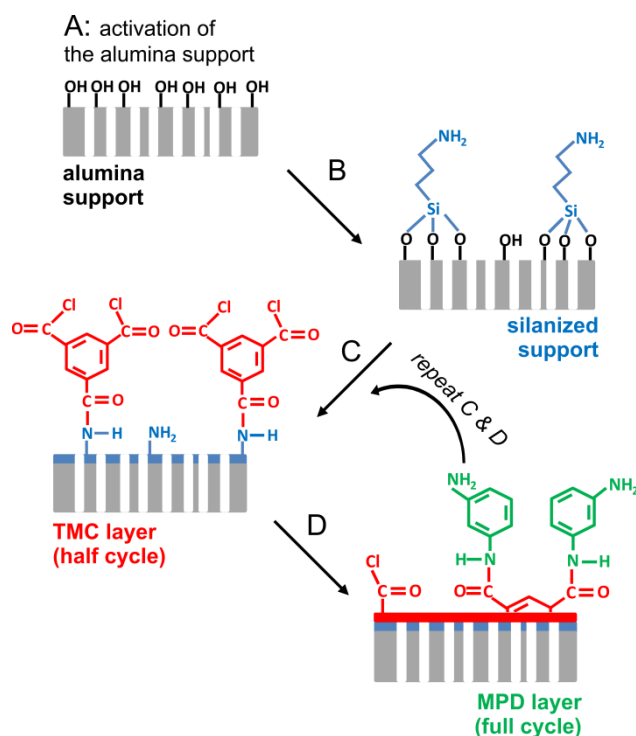


Figure 1. Schematic representation of the fabrication of oligoamide membranes by step-by-step assembly of covalently bound monomeric layers of MPD and TMC onto an aminated alumina ultrafiltration support. Reagents were: (B) APTES, (C) TMC in DCM, (D) MPD in toluene.

2.3 Characterization of supports and membranes

A Thermo-Nicolet 5700 apparatus was employed for Fourier transform infrared spectroscopy (FTIR) and for attenuated total reflectance (ATR)–FTIR analysis. The instrument is equipped with an ATR accessory containing a diamond crystal internal reflection element. The analysis was carried out with a resolution of 4 cm⁻¹ and samples were scanned 32 times in the wavenumber range between 750 and 3750 cm⁻¹ [29]. Thermogravimetric analyses (TGA) were performed with a Mettler TGA/SDTA 851 instrument between 20 and 650 °C at a heating rate of 10 °C min⁻¹ in air. Atomic force microscopy (AFM) was used to estimate the roughness characteristics of the membrane surfaces with a MFP-3D-Bio instrument (Asylum Research, Oxford Instruments) and employing an AC160TS probe (Olympus) in AC mode. AFM experiments involved the scanning of at least six different 5 × 5 μm areas for each membrane type. Samples were washed with ethanol and dried under nitrogen flow prior to measurement.

The surface and cross-sectional morphology of the membranes was analyzed through field emission scanning electron microscopy (FESEM). The instrument is the MERLIN model by ZEISS, equipped with a state-of-the-art GEMINILIS column, to ensure accurate control of spot and current [29]. The operational voltage was 5kV, except for the samples fabricated following 6.5 reaction cycles, for which the voltage was adjusted to 7.5 kV. Before analysis, samples were sputter-coated with a layer of chromium (8.0 nm) to prevent charging. The wettability of the membranes was determined via static contact angle measurements using a Krüss DSA-100 apparatus. The sessile drop method was chosen to measure the contact angle of deionized water in equilibrium mode and in several replicates [30].

X-ray photoelectron spectroscopy (XPS) characterization was carried out using a PHI 5000 Versaprobe scanning X-ray photoelectron spectrometer (monochromatic Al K-alpha X-ray source with 1486.6 eV energy, 15 kV voltage, and 1 mA anode current) on one sample for each cycle. A spot size of 100 μm was used to collect the photoelectron signal for both high resolution (HR) and

survey spectra. All samples were analyzed using a combined electron and argon ion gun neutralizer system to reduce the charging effect during the measurements. Spectra were analyzed using Multipak 9.6 software. All core-level peak energies were referenced to C1s peak at 284.5 eV and the background contribution in HR scans was subtracted by means of a Shirley function.

2.4 Evaluation of transport properties of supports and of final membranes

Filtrations were conducted at 20 °C in a dead-end stirred apparatus, Sterlitech HP4750, with effective membrane area of 14.6 cm². To measure water fluxes, the cell was initially pressurized with N₂ gas to reach a pressure drop of 15 psi for the experiments with pure porous alumina and 60 psi for both silanized supports and final membranes, monitored using a pressure gauge. At this pressure, the membranes were subjected to pre-compaction for 20 min; then, the pressure was reduced to 11, 9, 7, and 5 psi in the case of alumina supports, or to 87, 73, 60 and 44 psi in the case of silanized supports and final membranes. The flux at each pressure value was determined by collecting the permeate and by measuring the change in mass over time after the system reached steady state. The experiments were conducted using deionized water obtained from a Milli-Q water purification system. Water permeance, A , was calculated as the slope of pure water flux as a function of applied pressure, and is reported in LMH/bar ($\text{L m}^{-2} \text{h}^{-1} \text{bar}^{-1}$).

The nanofiltration rejection properties of the manufactured membrane were evaluated with a feed solution of 35 mM of mono and divalent salts, and samples were collected at 87 psi after pre-compaction at 100 psi of applied pressure. Samples were collected at steady state. The performance of the final membranes was compared with that of alumina supports and of silanized supports, evaluated using silica particles with permeate samples collected at 11 and 50 psi, respectively. A spectrophotometer was used to measure the absorbance of silica particles in both the feed solution (c_f) and the permeate solution (c_p) at a wavelength of 190 nm. Absorbance was linear with particle concentration in the range employed during the tests. To quantify salt rejection, the conductivity of both the feed (c_f) and the permeate solution (c_p) was determined using a

conductivity meter, with conductivity also showing a linear relationship with salt concentrations.

The observed rejection, R_o , was calculated as $R_o = 1 - \frac{c_p}{c_f}$. The solute permeance coefficient, B , was

determined by considering concentration polarization as $B = J_w \left(\frac{1 - R_o}{R_o} \right) \exp \left(-\frac{J_w}{k} \right)$ [31, 32], where

J_w is the permeate flux and k is the mass transfer coefficient, estimated using the Sherwood number and the empirical correlation for the exact geometry of the test cell valid for Reynolds number $\geq 3.2 \times 10^4$ [33].

3. Results and Discussion

3.1 Formation and Growth of the mLbL Assembly on Alumina Support

Figure 2 presents the results of the FTIR spectroscopic analyses performed on the materials at various stages of assembly and for increasing reaction cycles. The spectrum of the pristine alumina support shows appearance of characteristic peaks of Al_2O_3 at wavenumbers of roughly 1000 cm^{-1} . The amine-silanized membrane (blue line) had absorbance peaks near 1540 and 1500 cm^{-1} , typical of the deformation of C-H_2 and N-H_2 , respectively [34], which prove the successful anchoring of the APTES on the alumina surface. The peak at 1100 cm^{-1} may be attributed to the C-O-Si stretching band [34-36].

Moving upwards in the graphs, the red (half cycles, last reaction with TMC) and the green spectra (full cycles, last reaction with MPD) indicate successful formation and growth of the oligoamide layer. Figure 2b presents a zoomed view of the $1700\text{-}1500 \text{ cm}^{-1}$ wavenumber range for better visualization of the characteristic bands of polyamide. Growing peaks are attributed to amide I (C=O stretching, 1668 cm^{-1}), carbonyl groups (H-bonded C=O , 1610 cm^{-1}) and amide II (N-H bending, 1542 cm^{-1}). The same conclusions are drawn from ATR-FTIR spectra presented in the SI.

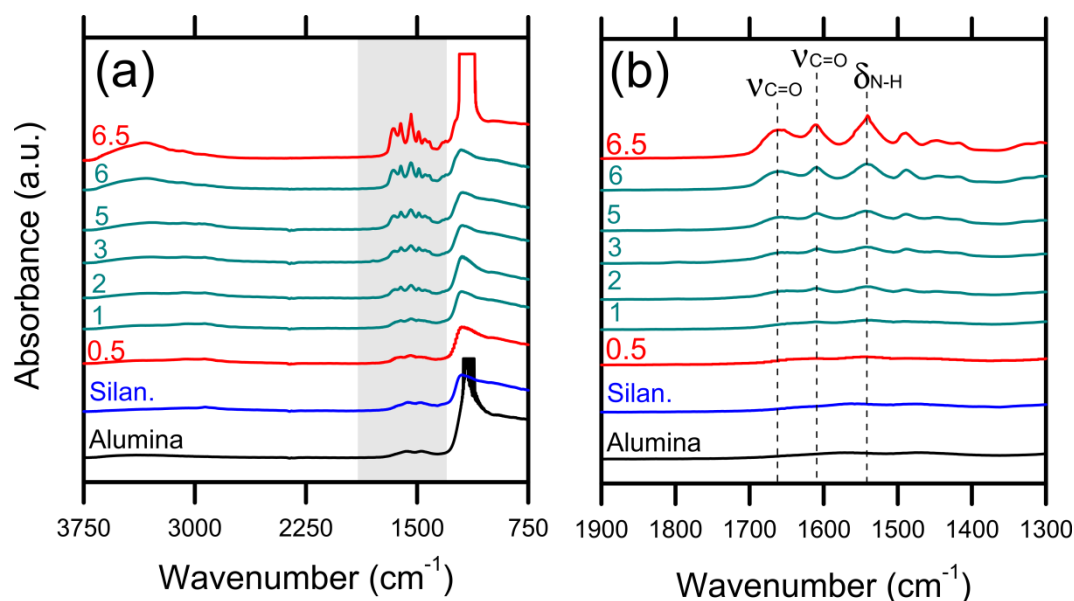


Figure 2. FTIR spectra of the membranes along the fabrication steps. a) entire spectra and b) zoomed view of the region of interest. The main peaks of interest are indicated. Bottom black curve denotes pure porous alumina; blue curve is the silanized alumina; red colors refer to intermediate half cycles oligoamide, while green colors to whole cycles.

XPS analysis corroborated the infrared spectroscopic results. Mostly aluminum and oxygen were found during measurements performed on the pristine alumina support (Figure S2). Also carbon was detected on these samples (~15%), due to residue from the electrochemical process of fabrication of these ultrafiltration membranes, as confirmed by the supplier. A significant amount (8-9%) of silicon was instead detected after silanization, suggesting the substantial extent of functionalization achieved during this step.

Figure 3 presents the ratios between C, O, and N elements in the film. Validation of the assembly procedure from the XPS spectra came from the distinctive trend of these ratios. TMC-terminated cycles had generally a higher oxygen-to-carbon ratio (O/C, 0.25-0.38) and a higher oxygen-to-nitrogen ratio (O/N, 2-2.6) than MPD-terminated oligoamide films (0.19-0.28 O/C and 1.25-1.7 O/N). The opposite trend was observed for N/C ratios, due to the diamine monomers completing the films fabricated by performing whole cycles. Typically, cross-linked polyamide films are evaluated based on the value of O/N ratio [37, 38]. However, in this study this ratio was always higher than 1, possibly due XPS probing of the underlying oxygen-rich alumina in locations of thin

organic coating. Therefore, we considered the N/C ratio as more representative of the extent of oligoamide cross-linking, and the slight increase in the N/C ratio along the assembly cycles indicated successful synthesis. Furthermore, this ratio was in the range 0.13-0.18, similar to values of 0.14-0.16 for commercial reverse osmosis membranes [39] and for polyamide or oligoamide films fabricated in the lab by both layer-by-layer techniques or classic interfacial polymerization [23, 40].

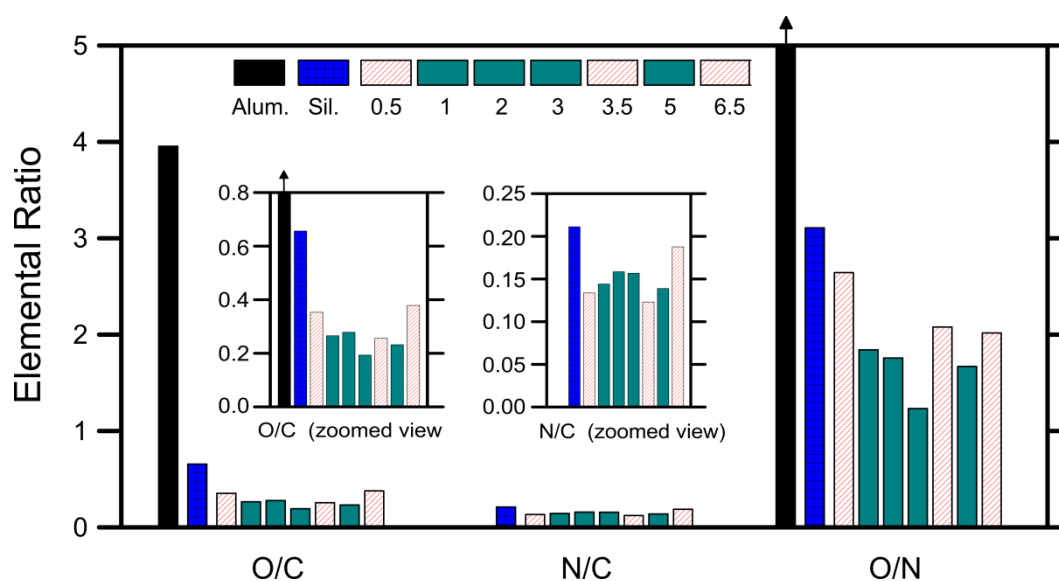


Figure 3. Atomic element ratio determined by X-ray photoelectron spectroscopy. Black bars denote pure porous alumina; blue bars are the silanized alumina; red patterned bars refer to intermediate half cycles oligoamide, while green solid bars to whole cycles.

Water contact angle measurements were in keeping with spectroscopic analyses by revealing the wettability of the various samples along the fabrication steps; see Figure 4. The alumina disk was highly wettable before modification with APTES and hydrophobic after silanization, with contact angles increasing from roughly 10° to above 80° . In the organic assembly stages, the values of the average contact angles followed a consistent trend as a function of the surface-exposed moiety: the surface of oligoamide ending at half cycles and exposing more carboxyl groups was generally more wettable (lower contact angles) than the corresponding integer cycles because aromatic-carboxyl groups are more hydrophilic than aromatic-amine groups; in addition, the aromatic ring in TMC

possesses more functionalities than in the MPD monomer. This fluctuating trend mirrors the data obtained from XPS analysis: higher density of oxygen-containing groups was reflected in higher surface wettability. However, the film growth resulted in contact angles progressively closer to those expected for polyamide membranes fabricated via classic interfacial polymerization, namely, $\sim 65^\circ$ [1]. Although the deposition of the two monomers may not be extensive during the initial assembly stages, all underlying layers contribute increasingly to reaching a surface energy similar to that of classic polyamide films for the final membrane.

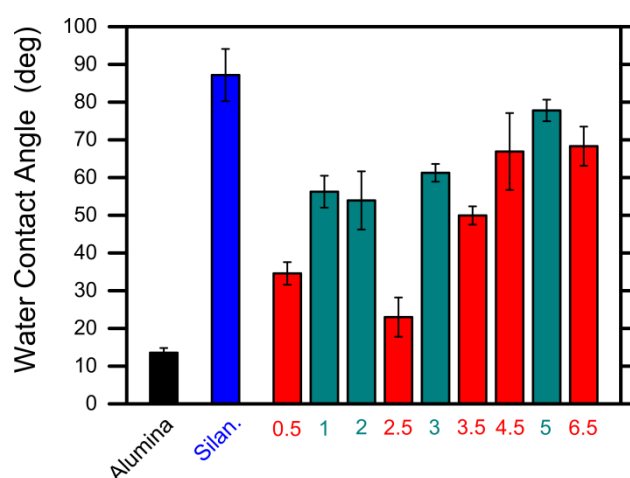


Figure 4. Evolution of the water droplet contact angle during the fabrication process: the black bar denotes pure porous alumina; the blue bar is the silanized alumina; red colors refer to intermediate half cycles oligoamide, while green colors to whole cycles.

3.2 Morphology of the Membrane as a Function of the Number of Reaction Steps

Figures 5 and 6 present SEM micrographs of the membranes along various reaction cycles. The porous alumina ultrafiltration support has average pore size of 20 nm at the active surface (Figure 5a); its active layer is thin (Figure 6a) and sits on top of well-ordered pores running across the thickness of the support. Organic films covering the alumina support surface can be observed following oligoamide assembly (Figures 5b-e; additional images are presented in Figure S3). The surface morphology of the layer appeared different from that of classic polyamide membranes fabricated via interfacial polymerization, which usually show a disordered and rough ridge-and-

valley structure [1], resulting instead in dendritic nanostructures. It is apparent that the organic layer quickly became denser as the number of reaction cycles increased. Inspection of the surface micrographs reveals also the increased presence of relatively large boil-like structures for membranes fabricated following higher numbers of reaction steps. A possible explanation for these results may be the non-uniform localized assembly of intermediate monomeric layers, which would result in the growth of non-homogeneous dendrimers. Another explanation may be the imperfect execution of intermediate washing steps between the monomeric deposition cycles: the presence of previously unreacted monomer would lead to localized formation of thicker nanostructures and possibly to polymerization of the monomers to form polyamide. Thermogravimetric (TGA) curves presented in Figure S5 suggest the presence of polyamide by showing values of mass loss that did not correlate with the number of reaction cycles. In fact, in the early stages (up to cycle 3), mass loss was lower than 1.5%. It increased significantly to 4% and almost 8% in cycles 5.5 and 6.5, respectively. We direct the reader to the Supporting Information for more details.

Further research should focus on improving the seeding of initial layers to be able to obtain more homogeneous membranes regardless of the number of reaction cycles. In accordance with the results discussed above, thicker organic films covered the backside pores of the membranes consisting of more monomeric layers, as shown in the SEM micrographs of the bottom surface of the membranes in Figure S4. Nevertheless, these films should not affect membrane performance as the greatest resistance to water flow would be exerted by the topmost dense layer.

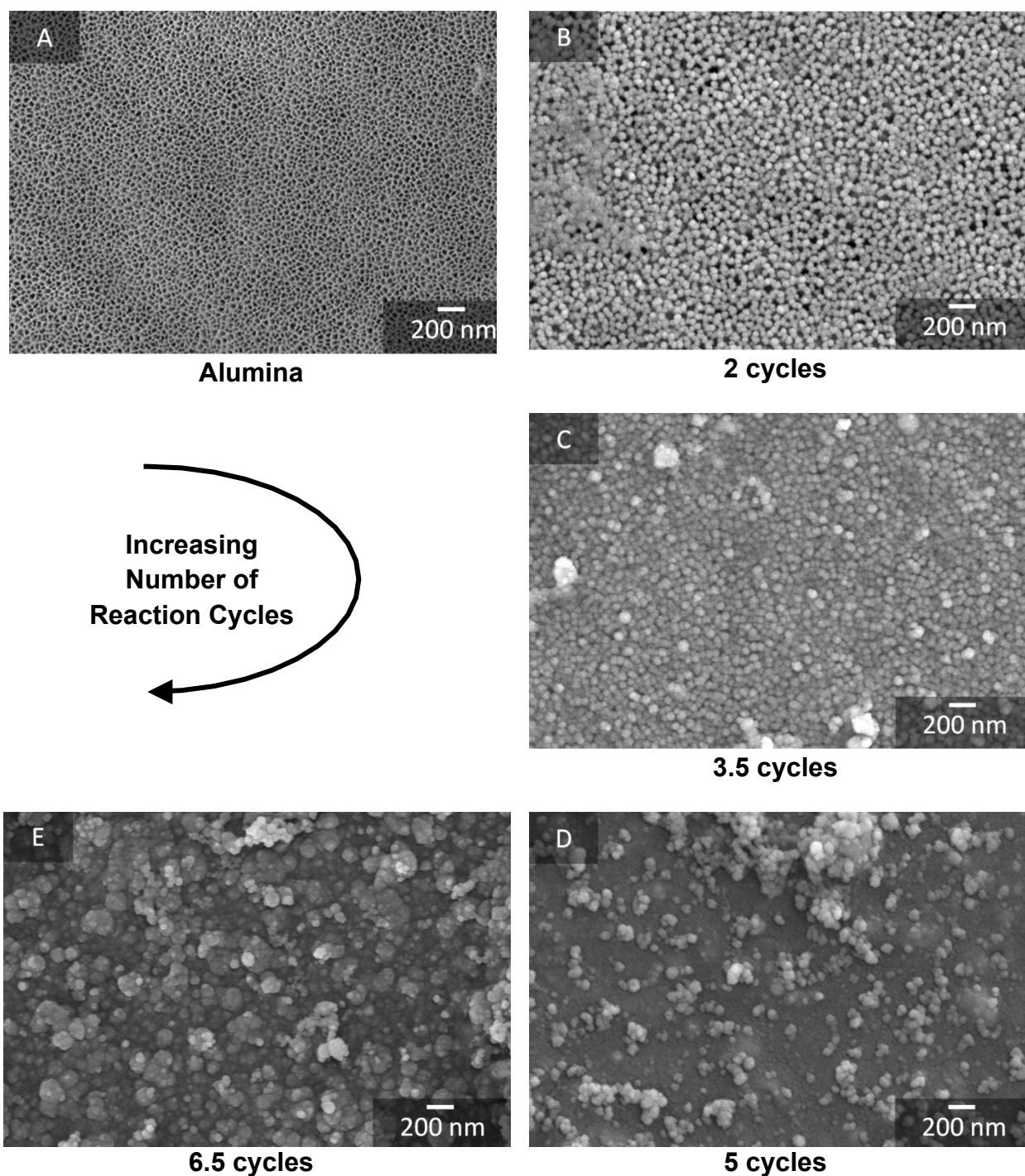


Figure 5. SEM micrographs of the membrane top surfaces along the cycles of layered synthesis. a) pure porous alumina; membranes obtained after b) 2 cycles; c) 3.5 cycles; d) 5 cycles; e) 6.5 cycles of fabrication.

Analysis of the membrane surface resulted in relatively smooth morphologies, as suggested by roughness parameters estimated with AFM and reported in Table 1. Average and RMS roughness values for membranes with different cycles of oligoamide were always below 30 nm and 40 nm, respectively, while maximum roughness was roughly 200 nm. Overall, these results are positive as

the observed roughness was lower than those found for polyamide membranes fabricated via classic interfacial polymerization, which are typically around 100 nm for average roughness and 300-400 nm for maximum roughness [1, 38]. Lowering surface roughness is one of the most important objectives of stepwise oligoamide fabrication, as a smoother surface is expected to reduce attachment of foulants [1]. In future investigations, it might be possible to test this hypothesis by performing fouling tests under filtration conditions.

Table 1. Transport performance and roughness characteristics of alumina supports and membranes along different fabrication steps.

	A ^a (LMH/bar)	R _o ^a of silica NPs 18 nm (%)	R _o ^a of silica NPs 32 nm (%)	R _o ^a of MgSO ₄ (%)	R _o ^a of NaCl (%)	RMS Roughness ^b (nm)	Average Roughness ^b (nm)	Max Roughness ^b (nm)
Alumina	1478 ± 118	81.2 ± 8.3	87.8 ± 4.8			45	35	181
Silanized	108 ± 25	91.6 ± 0.5	94.5 ± 0.5					
2 Cycles	14.2			17.1	17.5	32 ± 9	23 ± 7	181 ± 77
2.5 Cycles	6.1			46.4	32.4	29 ± 1	21 ± 1	232 ± 29
3.5 Cycles	2.71 ± 1.8			57.3 ± 11.3	44.0 ± 19.8	24 ± 3	18 ± 3	213 ± 30
4.5 Cycles	1.1			94.2	67.1	35 ± 3	25 ± 1	228 ± 65
5 Cycles	0.64			91.0	76.2 ± 2.1	22 ± 9	17 ± 6	108 ± 22
6.5 Cycles	0.65 ± 0.2			79.4 ± 4.1	56.4 ± 12.8	141 ± 5	108 ± 4	564 ± 109

^aStandard deviation values reported for parameters measured on different samples

^bStandard deviation values reported for data obtained in different locations on the same sample

The discussion has so far focused on the surface features of the membranes. However, another important aspect standing out in the cross-sectional images of Figure 6 is the probable presence of oligoamide inside the topmost pores of the support for all the reaction cycles. No evidence of increased thickness and density of oligoamide inside the pores can be positively detected as a function of number of reaction steps. These data may be somewhat limited by the influence of sample preparation or representativeness; however, it could conceivably be hypothesized that thicker organic films were obtained with higher number of reaction steps and that the oligoamide inside the support pores may influence the transport performance of the membranes.

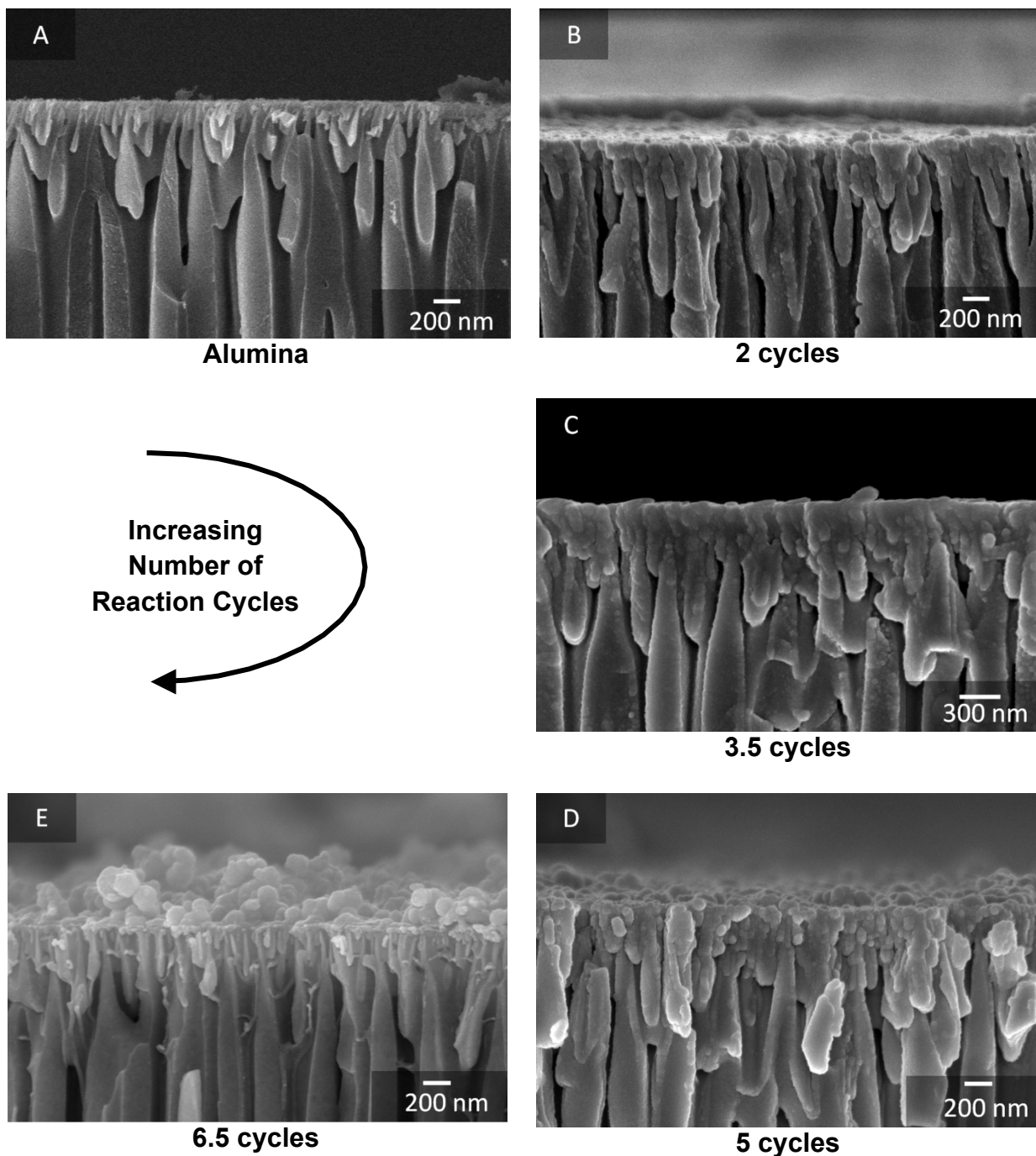


Figure 6. SEM micrographs of the membrane cross-section near the top surface along the cycles of layered synthesis. a) pure porous alumina; membranes obtained after b) 2 cycles; c) 3.5 cycles; d) 5 cycles; e) 6.5 cycles of fabrication.

3.3 Membrane Transport Performance as a Function of the Number of Reaction Steps

Table 1 collects some of the values of transport performance obtained for pristine alumina ultrafiltration supports, silanized supports, and the membranes obtained through different reaction cycles. The alumina support had a large permeability and was able to reject 88% of 32 nm

spherical nanoparticles, consistent with the morphology and high wettability of this active layer; see also Figure S6 of the SI. Average water fluxes were reduced after coupling the aminosilane, while the rejection of particles was slightly increased, demonstrating effective modification of the support surface with the more hydrophobic compound, which might also have partly closed the surface pores of the alumina active layer. Following anchoring of oligoamide, water permeance decreased and was further reduced as the oligoamide films were obtained by more steps of monomeric reaction (see Figure S7 of the Supporting Information). Specifically, observed water permeabilities changed from 14 LMH/bar for membranes fabricated with two reaction cycles, to lower than 1 LMH/bar for oligoamide comprising ten monomeric layers or more. Solute rejections had an opposite trend, except for the membrane fabricated by performing 6.5 reaction cycles. In the latter case, a dense organic layer coupled with the surface defects discussed in the previous section may be responsible for the decreased solute rejection observed in filtration tests. In general, the membranes performed within the nanofiltration range [31, 41], with the most promising results in terms of combination of water flux and salt rejection obtained for 3.5 and 4.5 reaction cycles.

Comparison with the transport performance of some commercial polymeric nanofiltration membranes is presented in Figure S8 of the Supporting Information.

The plot of selectivity, A/B , as a function of water permeance, A , in Figure 7 shows more clearly that the membranes fabricated in this study exhibited a permeance-rejection trade-off relationship (membranes obtained by 6.5 reaction steps represent outliers). An implication of these findings is the possibility to tune the membrane properties by adjusting the number of steps during fabrication, thus confirming the initial hypothesis driving this study. Further optimization of the fabrication procedure, such as better washing, reduction of the number of cycles, and optimization of monomer concentration and contact time, is expected to significantly improve the performance of the membrane obtained by mLbL assembly presented in this study [28].

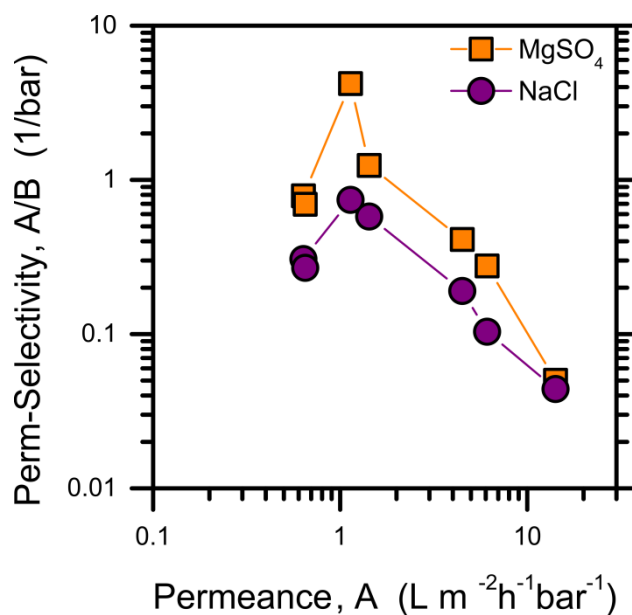


Figure 7. Experimental data showing correlation between water/solute perm-selectivity, A/B, and membrane permeance to water, A, for (orange squares) MgSO₄ and (purple circles) NaCl. Data points are connected by a solid line only to guide the eyes.

4. Conclusions

This project was undertaken to fabricate thin-film composite membranes by step-by-step synthesis (molecular layer-by-layer, mLbL) of oligoamide and to evaluate the effect of reaction steps on membrane performance. Layered oligoamide was assembled and covalently bound directly onto porous alumina supports, without the use of an anchoring intermediate polymeric layer. Fabrication was conducted by alternating layers of a triacid monomer (TMC) and a diamine monomer (MPD). Characterization techniques performed at various steps of film formation suggested that it grew sequentially; furthermore, analysis of the surface properties of the different membranes could detect the functionality of the monomer used in the latest reaction step. SEM analysis of the membrane cross-sections suggested the probable presence of the organic assembly both inside the topmost pores of the support and at its surface. The presence of surface defects increased with increased number of fabrication steps, but the surface morphologies were always smoother than those typically observed for commercial polyamide membranes, suggesting potentially reduced foulant

attachment during operation. Generally, membranes showed transport properties in the range of nanofiltration and governed by solution-diffusion. Strong positive correlation was observed between number of reactions steps and rejection capabilities, and the opposite for water permeance. The best combination of fluxes and rejection was found for membranes synthesized by performing 3.5 and 4.5 reaction cycles. In these cases, observed MgSO_4 rejections were roughly 60% and 90%, respectively, while observed NaCl rejections were approximately 45% and 65%. Future adjustments of the fabrication parameters are expected to further improve the membrane permeance and selectivity values. In particular, adequate washing of unreacted monomers between reaction steps appears to be critical to achieving a homogeneous assembly. In this study, the inorganic alumina represented a platform for the development of a robust mLbL strategy allowing covalent binding of the organic thin film to the support. However, use of inorganic supports may not be applicable for large scale production of membranes. Nevertheless, the approach proposed here is a step forward for the upcoming use of polymeric supports to fabricate commercially viable membranes for large-scale water-based filtrations. On the other hand, the chemical resistance of the alumina supports coupled with the transport performance observed in this study would allow effective use of the membranes for organic solvent nanofiltration or solvent-resistant nanofiltration, a promising area for future research.

Acknowledgements

This work was supported by project “StepPolyMem” within the Italy-Israel Scientific and Technological Cooperation funded by The Italian Ministry of Foreign Affairs and International Cooperation and by the Ministry of Science, Technology and Space of the State of Israel. We acknowledge Elena Dalla Vecchia, who assisted in the proofreading and language editing of the manuscript.

Appendix A. Supporting information

FTIR spectra of the membranes along the fabrication steps. Atomic composition (C, O, N, Si, Al) of the membranes along the fabrication steps. Additional SEM micrographs of the membrane top surfaces along the cycles of layered synthesis. SEM micrographs of the membrane bottom surfaces along the cycles of layered synthesis. Thermogravimetric analysis of the membranes along the fabrication steps. Measured pure water flux as function of applied pressure of three different alumina supports at 20 °C. Measured pure water flux as function of applied pressure of membranes along different reaction cycles at 20 °C. Comparison of separation performance of membranes fabricated in this study with some representative commercial polymeric nanofiltration membranes. (PDF)

References

- [1] M. Elimelech, W.A. Phillip, The Future of Seawater Desalination: Energy, Technology, and the Environment, *Science* 333 (2011) 712-717.
- [2] J.R. Werber, C.O. Osuji, M. Elimelech, Materials for next-generation desalination and water purification membranes, *Nat. Rev. Mater.* 1 (2016).
- [3] M.A. Shannon, P.W. Bohn, M. Elimelech, J.G. Georgiadis, B.J. Marinas, A.M. Mayes, Science and technology for water purification in the coming decades, *Nature* 452 (2008) 301-310.
- [4] W.J. Lau, S. Gray, T. Matsuura, D. Emadzadeh, J. Paul Chen, A.F. Ismail, A review on polyamide thin film nanocomposite (TFN) membranes: History, applications, challenges and approaches, *Water Res.* 80 (2015) 306-324.
- [5] P. Marchetti, M.F.J. Solomon, G. Szekely, A.G. Livingston, Molecular Separation with Organic Solvent Nanofiltration: A Critical Review, *Chem. Rev.* 114 (2014) 10735-10806.
- [6] P. Vandezande, L.E.M. Gevers, I.F.J. Vankelecom, Solvent resistant nanofiltration: separating on a molecular level, *Chem. Soc. Rev.* 37 (2008) 365-405.
- [7] R.J. Petersen, Composite Reverse-Osmosis and Nanofiltration Membranes, *J. Membr. Sci.* 83 (1993) 81-150.
- [8] J.E. Cadotte, R.S. King, R.J. Majerle, R.J. Petersen, Interfacial Synthesis in the Preparation of Reverse-Osmosis Membranes, *J. Macromol. Sci., Chem. A15* (1981) 727-755.
- [9] P.W. Morgan, S.L. Kwolek, Interfacial polycondensation .2. Fundamentals of polymer formation at liquid interfaces, *J. Polym. Sci., Part A: Polym. Chem.* 34 (1996) 531-559.
- [10] M.E. Tousley, D.L. Shaffer, J.H. Lee, C.O. Osuji, M. Elimelech, Effect of Final Monomer Deposition Steps on Molecular Layer-by-Layer Polyamide Surface Properties, *Langmuir* 32 (2016) 10815-10823.
- [11] V. Freger, Nanoscale Heterogeneity of Polyamide Membranes Formed by Interfacial Polymerization, *Langmuir* 19 (2003) 4791-4797.

- [12] D. Rana, T. Matsuura, Surface Modifications for Antifouling Membranes, *Chem. Rev.* 110 (2010) 2448-2471.
- [13] A. Giwa, N. Akther, V. Dufour, S.W. Hasan, A critical review on recent polymeric and nano-enhanced membranes for reverse osmosis, *RSC Adv.* 6 (2016) 8134-8163.
- [14] G.D. Kang, Y.M. Cao, Development of antifouling reverse osmosis membranes for water treatment: A review, *Water Res.* 46 (2012) 584-600.
- [15] W.J. Lau, A.F. Ismail, N. Misdan, M.A. Kassim, A recent progress in thin film composite membrane: A review, *Desalination* 287 (2012) 190-199.
- [16] K.P. Lee, T.C. Arnot, D. Mattia, A review of reverse osmosis membrane materials for desalination-Development to date and future potential, *J. Membr. Sci.* 370 (2011) 1-22.
- [17] A. Tiraferri, Y. Kang, E.P. Giannelis, M. Elimelech, Highly Hydrophilic Thin-Film Composite Forward Osmosis Membranes Functionalized with Surface-Tailored Nanoparticles, *ACS Appl. Mater. Interfaces* 4 (2012) 5044-5053.
- [18] A. Tiraferri, C.D. Vecitis, M. Elimelech, Covalent Binding of Single-Walled Carbon Nanotubes to Polyamide Membranes for Antimicrobial Surface Properties, *ACS Appl. Mater. Interfaces* 3 (2011) 2869-2877.
- [19] S. Badalov, C.J. Arnusch, Ink-jet printing assisted fabrication of thin film composite membranes, *J. Membr. Sci.* 515 (2016) 79-85.
- [20] S. Hermans, H. Mariën, E. Dom, R. Bernstein, I.F.J. Vankelecom, Simplified synthesis route for interfacially polymerized polyamide membranes, *J. Membr. Sci.* 451 (2014) 148-156.
- [21] H. Mariën, L. Bellings, S. Hermans, I.F.J. Vankelecom, Sustainable Process for the Preparation of High-Performance Thin-Film Composite Membranes using Ionic Liquids as the Reaction Medium, *ChemSusChem* 9 (2016) 1101-1111.
- [22] H. Marien, L. Bellings, S. Hermans, I.F.J. Vankelecom, Sustainable Process for the Preparation of High-Performance Thin-Film Composite Membranes using Ionic Liquids as the Reaction Medium, *ChemSusChem* 9 (2016) 1101-1111.

- [23] Z. Steiner, J. Miao, R. Kasher, Development of an oligoamide coating as a surface mimetic for aromatic polyamide films used in reverse osmosis membranes, *Chem. Commun.* 47 (2011) 2384-2386.
- [24] W. Ying, R. Kumar, M. Herzberg, R. Kasher, Diminished Swelling of Cross-Linked Aromatic Oligoamide Surfaces Revealing a New Fouling Mechanism of Reverse-Osmosis Membranes, *Environ. Sci. Technol.* 49 (2015) 6815-6822.
- [25] D.H. Wu, Y.F. Huang, S.C. Yu, D. Lawless, X.S. Feng, Thin film composite nanofiltration membranes assembled layer-by-layer via interfacial polymerization from polyethylenimine and trimesoyl chloride, *J. Membr. Sci.* 472 (2014) 141-153.
- [26] W. Choi, J.E. Gu, S.H. Park, S. Kim, J. Bang, K.Y. Baek, B. Park, J.S. Lee, E.P. Chan, J.H. Lee, Tailor-Made Polyamide Membranes for Water Desalination, *ACS Nano* 9 (2015) 345-355.
- [27] W. Choi, S. Jeon, S.J. Kwon, H. Park, Y.-I. Park, S.-E. Nam, P.S. Lee, J.S. Lee, J. Choi, S. Hong, Thin Film Composite Reverse Osmosis Membranes Prepared via Layered Interfacial Polymerization, *J. Membr. Sci.* In Press (2017).
- [28] J.E. Gu, S. Lee, C.M. Stafford, J.S. Lee, W. Choi, B.Y. Kim, K.Y. Baek, E.P. Chan, J.Y. Chung, J. Bang, J.H. Lee, Molecular Layer-by-Layer Assembled Thin-Film Composite Membranes for Water Desalination, *Adv. Mater.* 25 (2013) 4778-4782.
- [29] L.C. Capozzi, F.M. Mehmood, M. Giagnorio, A. Tiraferri, M. Cerruti, M. Sangermano, Ultrafiltration Membranes Functionalized with Polydopamine with Enhanced Contaminant Removal by Adsorption, *Macromol. Mater. Eng.* In Press (2017).
- [30] A. Amelio, L. Loise, R. Azhandeh, S. Darvishmanesh, V. Calabro, J. Degreve, P. Luis, B. Van der Bruggen, Purification of biodiesel using a membrane contactor: Liquid-liquid extraction, *Fuel Process. Technol.* 142 (2016) 352-360.
- [31] R. Baker, *Membrane Technology and Applications*, 2nd edition ed., Wiley, 2004.

- [32] A. Tiraferri, N.Y. Yip, A.P. Straub, S.R.V. Castrillon, M. Elimelech, A method for the simultaneous determination of transport and structural parameters of forward osmosis membranes, *J Membrane Sci* 444 (2013) 523-538.
- [33] C.K. Colton, K.A. Smith, Mass-Transfer to a Rotating Fluid .2. Transport from Base of an Agitated Cylindrical Tank, *Aiche J* 18 (1972) 958-&.
- [34] A.R. Erdogan, I. Kaygusuz, C. Kaynak, Influences of aminosilanization of halloysite nanotubes on the mechanical properties of polyamide-6 nanocomposites, *Polym. Compos.* 35 (2014) 1350-1361.
- [35] J. Amici, M.U. Kahveci, P. Allia, P. Tiberto, Y. Yagci, M. Sangermano, Polymer grafting onto magnetite nanoparticles by "click" reaction, *J. Mater. Sci.* 47 (2012) 412-419.
- [36] S.H. Hyun, S.Y. Jo, B.S. Kang, Surface modification of gamma-alumina membranes by silane coupling for CO₂ separation, *J. Membr. Sci.* 120 (1996) 197-206.
- [37] V.T. Do, C.Y.Y. Tang, M. Reinhard, J.O. Leckie, Degradation of Polyamide Nanofiltration and Reverse Osmosis Membranes by Hypochlorite, *Environ. Sci. Technol.* 46 (2012) 852-859.
- [38] C.Y.Y. Tang, Y.N. Kwon, J.O. Leckie, Effect of membrane chemistry and coating layer on physiochemical properties of thin film composite polyamide RO and NF membranes I. FTIR and XPS characterization of polyamide and coating layer chemistry, *Desalination* 242 (2009) 149-167.
- [39] O. Akin, F. Temelli, Probing the hydrophobicity of commercial reverse osmosis membranes produced by interfacial polymerization using contact angle, XPS, FTIR, FE-SEM and AFM, *Desalination* 278 (2011) 387-396.
- [40] M.J. Ariza, J. Benavente, E. Rodriguez-Castellon, L. Palacio, Effect of hydration of polyamide membranes on the surface electrokinetic parameters: Surface characterization by X-ray photoelectronic spectroscopy and atomic force microscopy, *J. Colloid Interface Sci.* 247 (2002) 149-158.

[41] W.S. Ang, A. Tiraferri, K.L. Chen, M. Elimelech, Fouling and cleaning of RO membranes fouled by mixtures of organic foulants simulating wastewater effluent, *J. Membr. Sci.* 376 (2011) 196-206.

SUPPORTING INFORMATION

Fabrication of Nanofiltration Membranes via Stepwise Assembly of Oligoamide on Alumina Supports: Effect of Number of Reaction Cycles on Membrane Properties

Antonio Amelio^a, Marco Sangermano^b, Roni Kasher^c, Roy Bernstein^c, Alberto
Tiraferri^{a,*}

*^aDepartment of Environment, Land and Infrastructure Engineering (DIATI), Politecnico di Torino, Corso
Duca degli Abruzzi 24, 10129, Torino, Italy*

*^bDepartment of Applied Science and Technology (DISAT), Politecnico di Torino, Corso Duca degli Abruzzi
24, 10129, Torino Italy*

*^cDepartment of Desalination and Water Treatment, Zuckerberg Institute for Water Research, Jacob
Blaustein Institute for Desert Research, Ben-Gurion University of the Negev, Midreshet-Ben Gurion, Sede
Boqer, Israel*

*alberto.tiraferri@polito.it; Corso Duca degli Abruzzi 24, 10129, Torino, Italy; Tel. +390110907628, Fax:
+390110907699

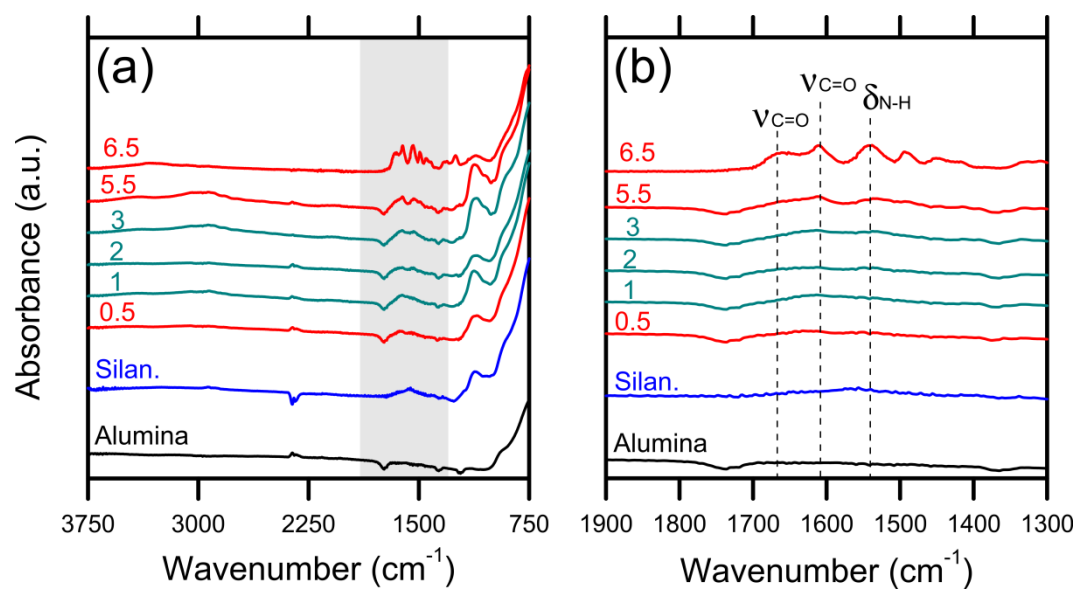


Figure S1. ATR-FTIR spectra of the membranes along the fabrication steps. a) entire spectra and b) zoomed view of the region of interest. The main peaks of interest are indicated. Bottom black curve denotes pure porous alumina; blue curve is the silanized alumina; red colors refer to intermediate half cycles oligoamide, while green colors to complete cycles.

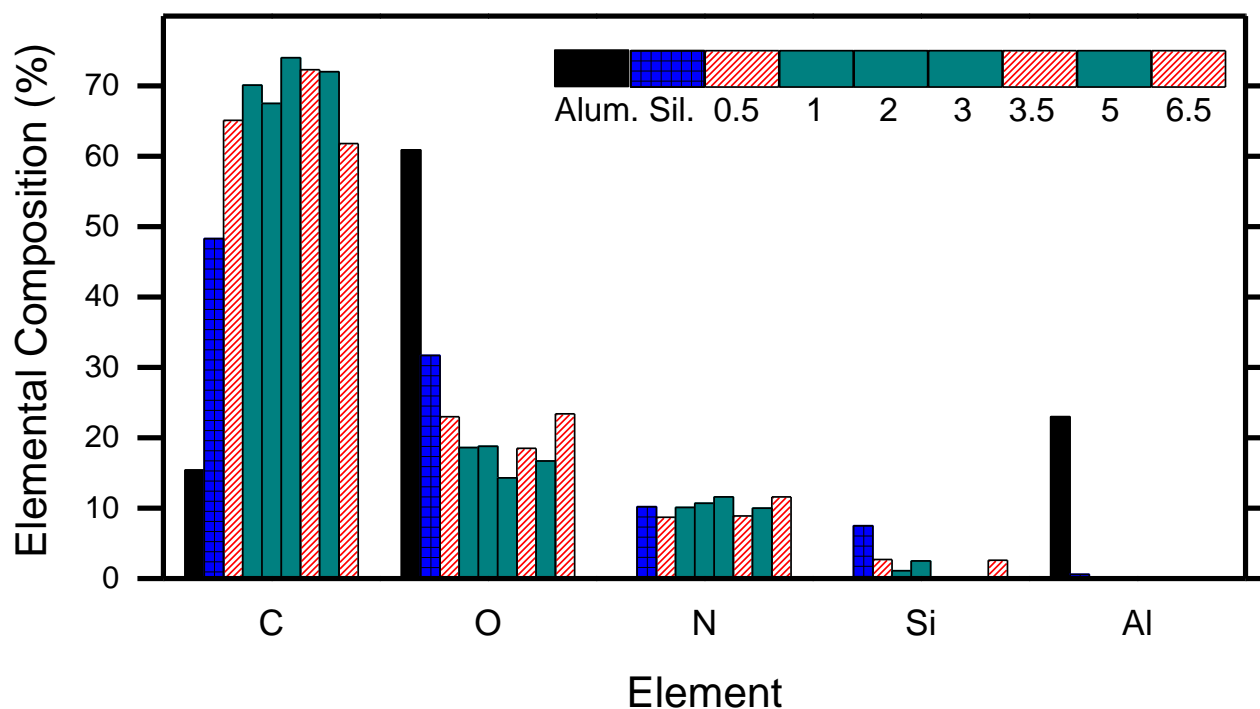


Figure S2. Atomic composition of the membrane along the fabrication steps. Black bars denote pure porous alumina; blue bars are the silanized alumina; red patterned bars refer to intermediate half cycles oligoamide, while green solid bars to whole cycles.

Figure S2 displays the C, O, and N composition. In the first stages of membrane fabrication, the atomic percent of carbon increased due to the presence of the alkyl backbone in APTES and of carbon-rich rings in TMC and MPD, while the relative amount of oxygen decreased as alumina was progressively covered by the oligoamide assembly. After the first few steps of OA growth, the atomic percent of carbon remained roughly constant and close to 70%, which is within the range of values typical for polyamide membranes [1, 2]. Validation of the assembly procedure from the XPS spectra came from the distinctive trend of O and N detected along the half and full reaction cycles: the relative amount of oxygen was usually higher for the half cycles (TMC as last reacting monomer), while nitrogen was relatively more abundant for the full cycles, due to the diamine monomers completing the film.

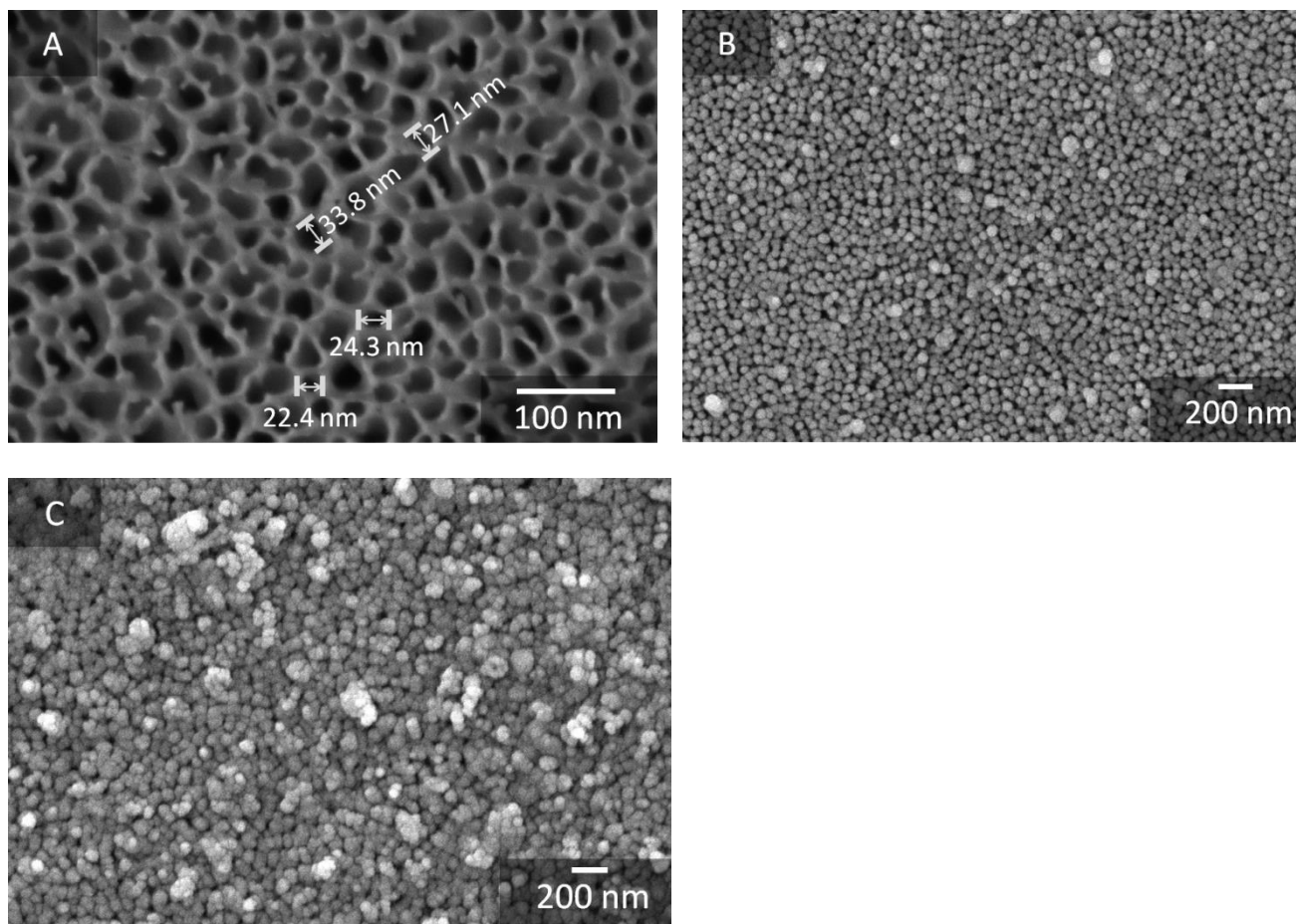


Figure S3. Additional SEM micrographs of the membrane top surfaces along the cycles of layered synthesis. a) pure porous alumina; membranes obtained after b) 2.5 cycles; c) 4.5 cycles of fabrication. Estimate measurements of some pore size were made using ImageJ software.

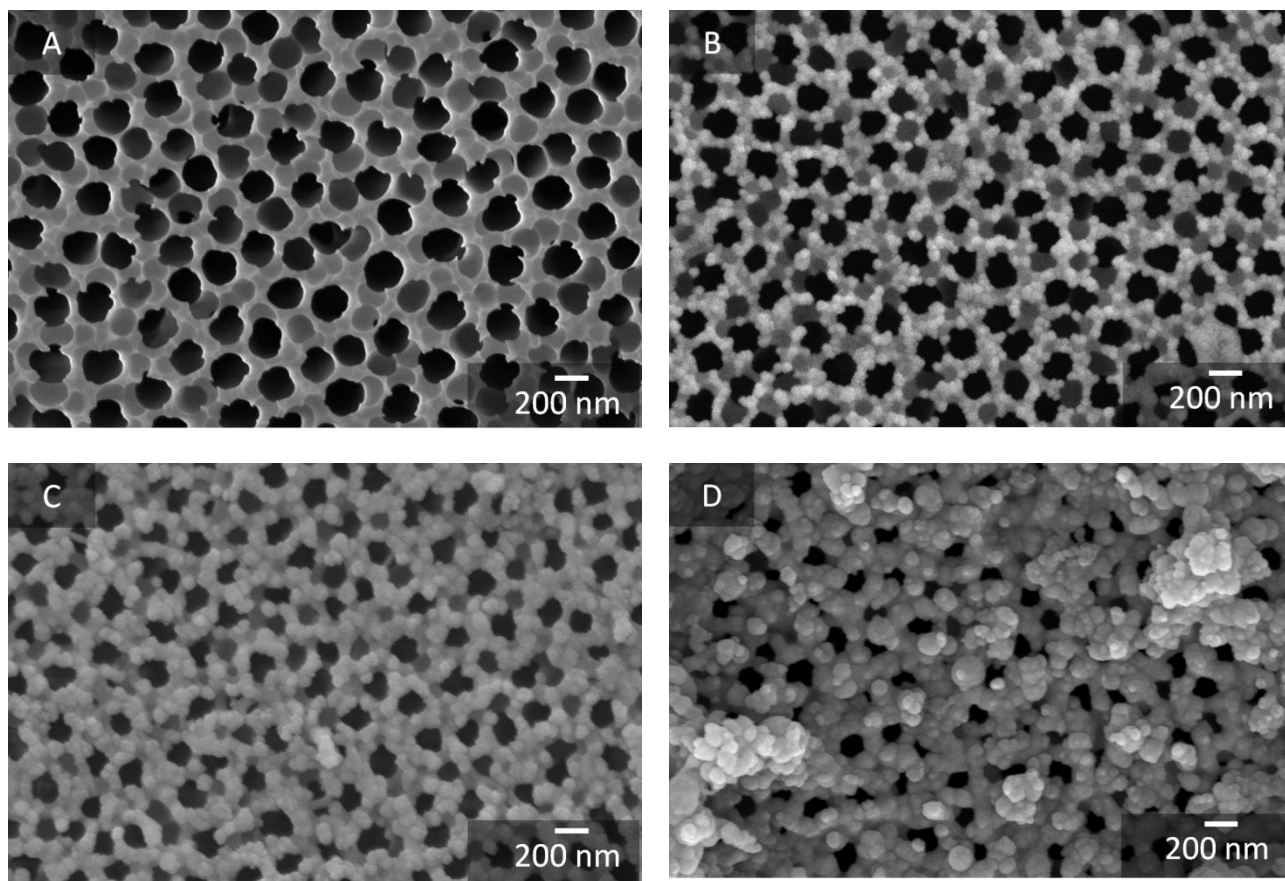


Figure S4. SEM micrographs of the membrane bottom surfaces along the cycles of layered synthesis. a) pure porous alumina; membranes obtained after b) 2 cycles; c) 5 cycles; d) 6.5 cycles of fabrication.

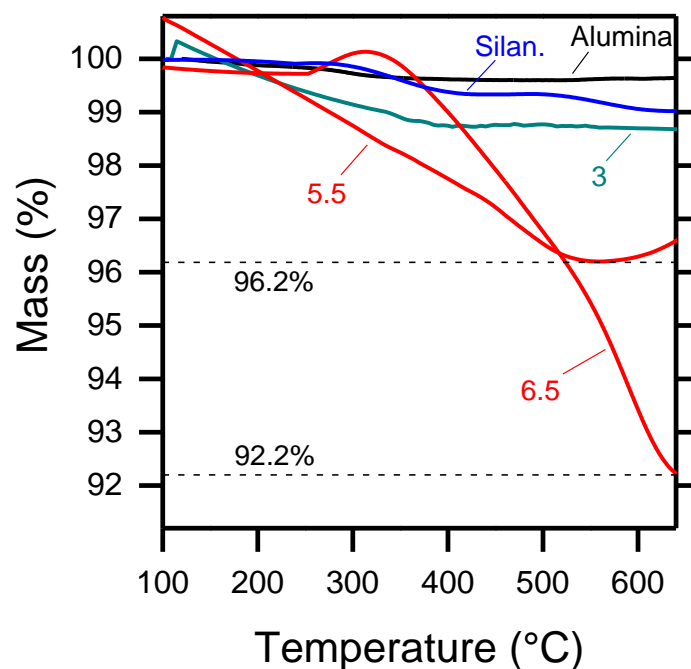


Figure S5. Results from thermogravimetric analysis (TGA) of the membrane along the fabrication steps: black curve denotes pure porous alumina; blue curve is the silanized alumina; red colors refer to intermediate half cycles oligoamide, while green colors to whole cycles.

The thermogravimetric curves decrease starting at a temperature of 400°C, suggesting that the samples were thermally stable up to this value [3]. The data suggest that almost 8% of the sample corresponding to the final membrane, obtained after 6.5 reaction cycles, consisted of organic material attributable mostly to OA. However, the increased weight loss along the cycles of membrane fabrication was not proportional to the number of cycles. Weight loss was negligible for the pristine porous alumina filter, roughly 1% for silanized supports, only 1.5% after three full assembly cycles (cycle 3, green line), and approximately 4% just prior to the assembly of the last two monomeric layers (cycle 5.5, red line). This trend supports the conclusion suggested by SEM analysis that the sequential monomeric reactions gave rise to dendrimeric structures which by definition became more and more dense and thick along the several cycles. Also, polyamide defects observed at increased number of reaction cycles contributed to a significantly larger mass loss in TGA measurements.

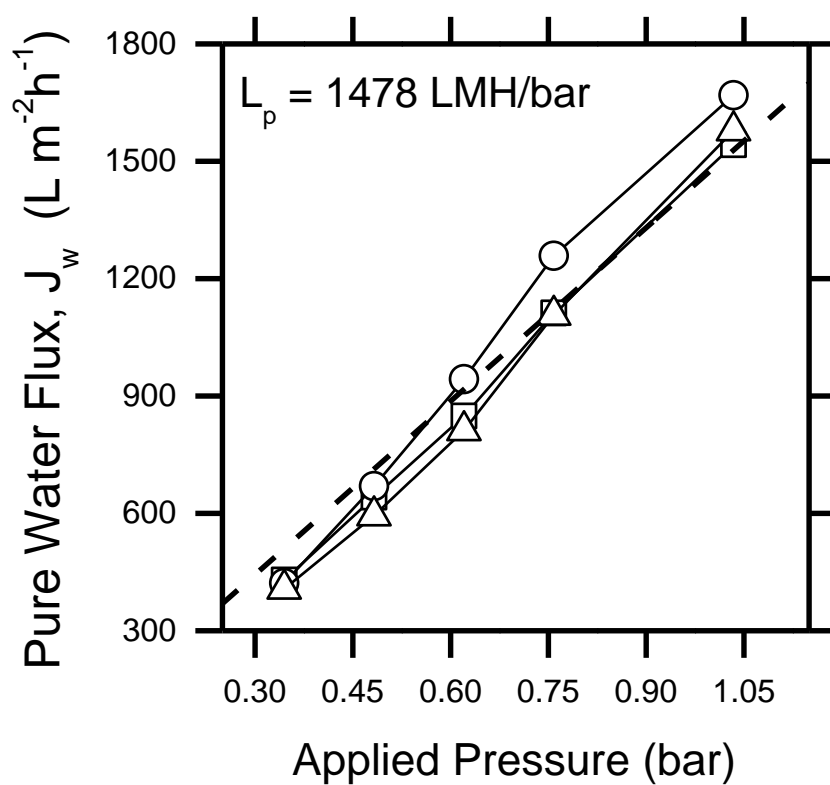


Figure S6. Measured pure water flux as function of applied pressure of three different alumina supports at 20 °C. Black dotted line denotes the concatenated fitting used to estimate average water permeability, L_p , reported on the top left corner.

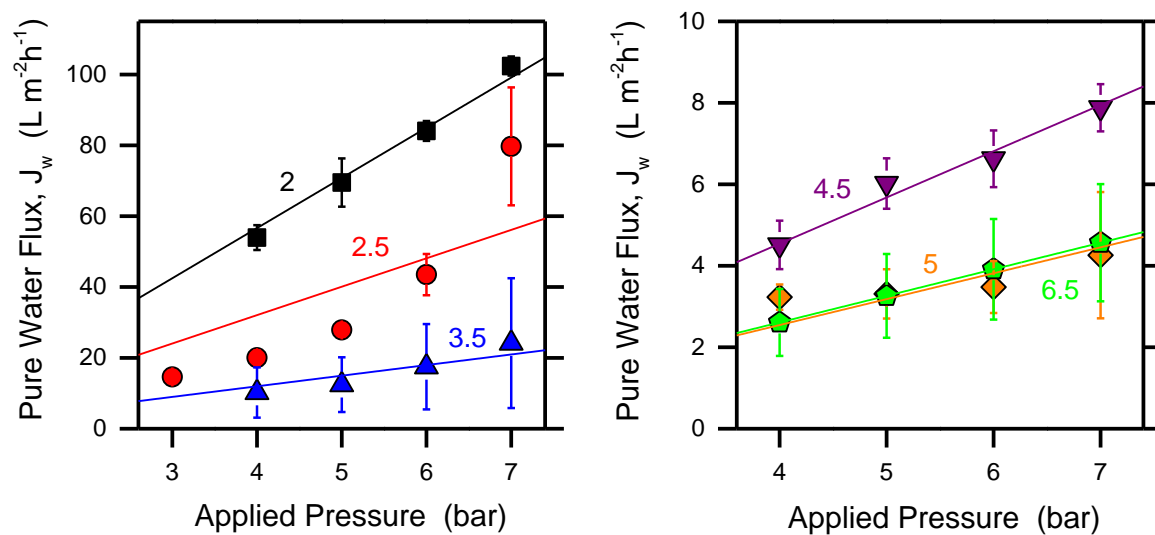


Figure S7. Measured pure water flux as function of applied pressure at 20 °C for membranes along different reaction cycles (indicated). Solid lines denote the fitting used to estimate average water permeance.

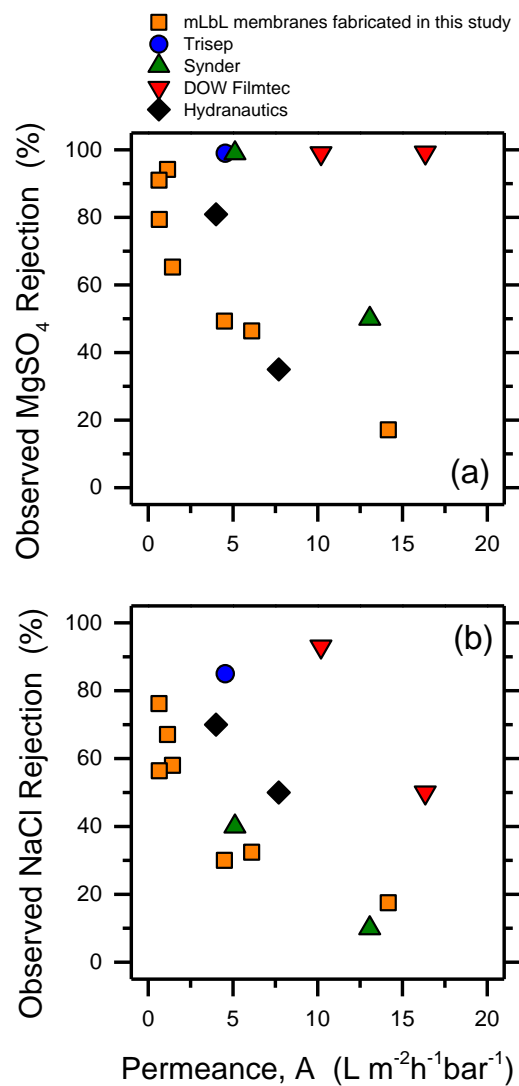


Figure S8. Comparison of separation performance of membranes fabricated in this study with some representative commercial polymeric nanofiltration membranes. Rejection of (a) MgSO_4 or (b) NaCl plotted as a function of permeance, A. Please note that the data for commercial membranes is a combination of values obtained from specification sheets and laboratory experiments.

References

- [1] W. Choi, J.E. Gu, S.H. Park, S. Kim, J. Bang, K.Y. Baek, B. Park, J.S. Lee, E.P. Chan, J.H. Lee, Tailor-Made Polyamide Membranes for Water Desalination, *ACS Nano* 9 (2015) 345-355.
- [2] Y.N. Kwon, C.Y. Tang, J.O. Leckie, Change of chemical composition and hydrogen bonding behavior due to chlorination of crosslinked polyamide membranes, *J. Appl. Polym. Sci.* 108 (2008) 2061-2066.
- [3] J. Charles, G.R. Ramkumaar, S. Azhagiri, S. Gunasekaran, FTIR and Thermal Studies on Nylon-66 and 30% Glass Fibre Reinforced Nylon-66, *E-J. Chem.* 6 (2009) 23-33.